

# Interfacial Fracture Toughness of Fiber Reinforced Titanium Matrix Composites by Push out Test

Sun Qing<sup>1,2</sup>, Yang Yanqing<sup>1</sup>, Luo Xian<sup>1</sup>, Zhang Rongjun<sup>1</sup>, Huang Bin<sup>1</sup>, Xue Chunling<sup>1</sup>

<sup>1</sup>State Key Laboratory of Solidification Processing, Northwestern Polytechnical University, Xi'an 710072, China; <sup>2</sup>Baoji University of Arts and Sciences, Baoji 721000, China

**Abstract:** The model for single fiber push-out test was developed to evaluate the fracture toughness  $G_{IIc}$  of the fiber/matrix interface in titanium alloys reinforced by SiC monofilaments. Theoretical solution to  $G_{IIc}$  was obtained from fracture mechanics, and the effects of several key factors such as the applied stress needed for crack advance, crack length, and interfacial frictional shear stress were discussed. The predictions by the model were compared with the previous finite element analysis results for the interfacial toughness of the composites including Sigma1240/Ti-6-4, SCS/Ti-6-4, SCS/Timetal 834 and SCS/Timetal 21s. The results show that the model can reliably predict the interfacial toughness of the titanium matrix composites, in which interfacial debonding usually occurs at the bottom of the samples.

**Key words:** titanium matrix composites (TMCs); interfacial fracture toughness; push-out test; shear-lag approach

SiC fiber-reinforced titanium-matrix composites (TMCs) can be widely used in aerospace and automobile industries due to their low density, high performance, high specific strength and stiffness at room and elevated temperatures<sup>[1-7]</sup>. The behavior of fiber/matrix interfaces plays an important role in the successful applications of these composites. Push-out test has been introduced as an important experimental techniques for characterizing the interfacial performance of this class of composites owing to its simplicity of preparing the specimen and conducting the experiment. Typical push-out test curve and the schematic of the test is shown in Fig.1<sup>[8-10]</sup>. In Fig.1b, the abscissa represents the length of fiber, the ordinate represents the load  $P$ ,  $P_i$  represents an initial debonding load,  $P_{max}$  represents the maximum external load,  $P_d$  is any load in between  $P_i$  and  $P_{max}$ , and  $P_{fr}$  is the applied load which is used to overcome frictional sliding after complete debonding.

Push-out test at first has been widely used in the study of interfaces in ceramic matrix composites (CMCs)<sup>[9,11]</sup>. Compared

with the CMCs, TMCs have relatively high bond strength and residual clamping stresses at the interface, which require thinner slices of composites so that SiC fibers can be moved before the indenter fractures or the fiber crushes<sup>[12]</sup>. Moreover, for almost all of this thin slice push-out test of TMCs, it has been observed that the interfacial crack initiates and propagates from the bottom of the specimen due to thermal residual stresses at the interface<sup>[8,12-15]</sup>. This crack initiation in TMCs is completely different from CMCs where crack initiates from the top of the specimen. Obviously, the failure mechanism of the push-out in TMCs and CMCs is different, and it is therefore needed to develop theoretical models for TMCs in order to understand their interfacial mechanical properties.

The fracture mechanics approach is very attractive in the analysis of the push-out problem because it can address the crack propagation during the process of the fiber push-out and energies of the interfacial debonding<sup>[16-19]</sup>. Majumdar<sup>[20]</sup> proposed that interfacial fracture toughness is the change in strain energy of the system and the work done by the loading system due to crack propagation. Following

Received date: October 23, 2016

Foundation item: Program of Introducing Talents of Discipline to Universities (B08040); National Nature Science Foundation of China (51071122, 51271147, 51201134); Fundamental Research Funds for the Central Universities (3102014JCQ01023); Foundation of the Doctoral Scientific Research of Baoji University of Arts and Sciences (ZK2017020, ZK2017022)

Corresponding author: Yang Yanqing, Professor, School of Materials Science, Northwestern Polytechnical University, Xi'an 710072, P. R. China, Tel: 0086-29-88460499, E-mail: yqyang@nwpu.edu.cn

Copyright © 2017, Northwest Institute for Nonferrous Metal Research. Published by Elsevier BV. All rights reserved.

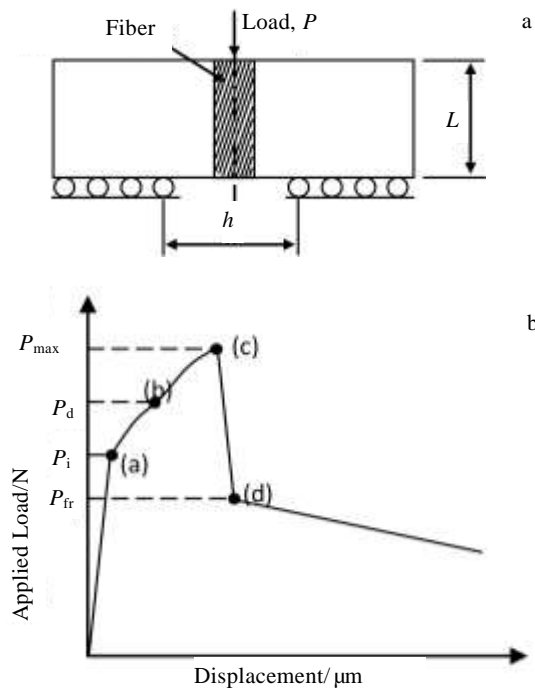


Fig.1 Single fiber push-out test: (a) the schematic<sup>[9]</sup> and (b) typical load-displacement curve<sup>[8]</sup>

Majumdar's approach<sup>[20]</sup>, Kalton<sup>[21]</sup> took into account the work done in frictional sliding at the interface. All above works are for situations of interfacial debonding on the top of the samples. However, for TMCs, the crack is likely to have propagated from bottom to top.

In this paper, an analytical model has been developed for the situations where crack propagates from the bottom face during push-out test. The paper is arranged as follows. In section 2, the solution to  $G_{IIC}$  is deduced based on Kalton's basic energy balance equation. In section 3, several key factors that determine the critical applied stress necessary for crack growth, such as crack length and the interfacial frictional shear stress, are discussed based on the models. In section 4,  $G_{IIC}$  of the composites Sigma1240/Ti-6-4, SCS/Ti-6-4, SCS/Timetal 834 and SCS/Timetal 21s are calculated by incorporating the load/displacement curves of push-out test and the thermal residual stresses to validate the prediction of the present theoretical model.

## 1 Analysis of Interfacial Fracture Toughness

### 1.1 Synopsis for the analytical models

Fig.2 shows the geometric representation of the fiber/matrix cylinder model, where  $r_f$  is fiber radius and  $L$  is thickness of specimen. At the top end of the specimen,  $z = 0$ , the fiber is loaded by a force  $P$ , and at the other end,  $z = L$ , the fiber is free and the matrix is fixed. An interfacial

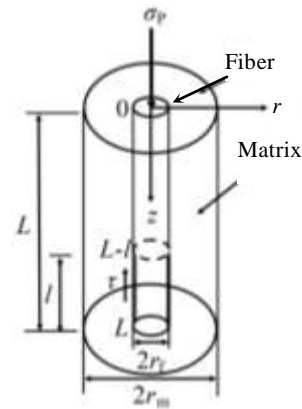


Fig.2 Idealized fiber push-out model

crack is assumed to initiate at  $z = L$  (bottom) surface and propagates from the bottom face to the top face. It is also assumed that the stresses within the matrix and the compliance of the matrix are neglected, and the stresses within the fiber are independent of radial location. The interfacial frictional shear stress  $\tau$  follows Coulomb frictional law:

$$\tau = \tau_0 + \mu \sigma_{r, \Delta T} \quad (1)$$

where  $\tau_0$  is the constant friction,  $\mu$  is the coefficient of friction and  $\sigma_{r, \Delta T}$  is the radial thermal residual stress. This relation was used by Jero<sup>[22]</sup> and Mackin<sup>[23]</sup> in earlier work, and later was adopted widely by many other workers<sup>[21,24]</sup>.

The basic energy balance equation used here is<sup>[21]</sup>:

$$G_{IIC} = \frac{dU_{ex}}{dA} - \frac{dU_{se}}{dA} - \frac{dU_{fr}}{dA} \quad (2)$$

where  $dA$  is the incremental increase in crack surface area,  $dU_{ex}$  is the work done by the loading system,  $dU_{se}$  is the change in strain energy of the system due to crack advance, and  $dU_{fr}$  is the work done in frictional sliding at the interface. All strain energies are neglected in the matrix due to their small values<sup>[21]</sup>.

### 1.2 Expression of interfacial fracture toughness

It is assumed that the interface bonds perfectly at the two free end surface. In order to analyze the progressive debonding portion of the load/displacement curve of push-out test, the specimen is divided into three different regions, namely, a debonding region I ( $L-l \leq z \leq L$ ), a crack tip region II ( $L-l \leq z \leq l_1$ ) and a bonded region III ( $l_1 \leq z \leq 0$ ), as shown in Fig.3. By the shear-lag approach, the axial equilibrium equation in the fiber is<sup>[24]</sup>:

$$\frac{d\sigma_f(z)}{dz} = -\frac{2\tau}{r_f} \quad (3)$$

where  $\sigma_f(z)$  is the axial stress in the fiber.

In region I, interfacial debonding has occurred, and the axial stress in the fiber comes from only the frictional sliding resistance at the interface since this region locates the bottom

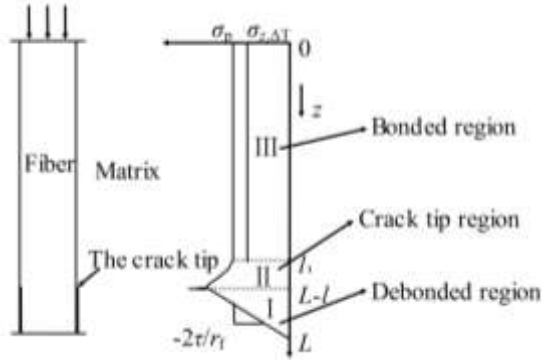


Fig.3 Schematic representation of the axial stress in the fiber during push-out test

end of the specimen. The axial stress in the fiber is obtained by integrating equation (3) from  $L$  to  $z$  and is given by

$$\sigma_1(z) = \frac{2\tau(L-z)}{r_f} \quad (4)$$

The axial stress in the fiber is different from that of crack initiation at the top of the specimen in this region.

In region II, the axial stress is not well-defined in the fiber because its distribution shows singularity due to the effect of crack tip. Moreover, the region is very small and any effect of crack length and  $P$  on this distribution is neglected<sup>[20,21]</sup>.

In region III, it is assumed that the axial stress in the fiber is independent of radial location and axial location. Combining the applied stress  $\sigma_p$  and the thermal residual stress yields:

$$\sigma_{III}(z) = \sigma_p - \sigma_{z,\Delta T} \quad (5)$$

where  $\sigma_p$  is the applied stress induced by load  $P$ , and  $\sigma_{z,\Delta T}$  is the axial thermal residual stress in the fiber. It is seen from equations (4) and (5) that the axial stress in the fiber falls from  $\sigma_p - \sigma_{z,\Delta T}$  at the top end to zero at the bottom end of the specimen.

The expressions of  $dU_{ex}$ ,  $dU_{se}$  and  $dU_{fr}$  in equation (2) can be obtained from equations (4) and (5), and the process is detailed in Appendix. These terms can be expressed as follows:

$$\frac{dU_{ex}}{dA} = \frac{r_f}{2E_f} \sigma_{P,c} (\sigma_{P,c} - \sigma_{z,\Delta T} - \frac{2\tau l}{r_f}) \quad (6)$$

$$\frac{dU_{se}}{dA} = \frac{r_f}{4E_f} [(\sigma_{P,c} - \sigma_{z,\Delta T})^2 - \frac{4\tau^2 l^2}{r_f^2}] \quad (7)$$

$$\frac{dU_{fr}}{dA} = \frac{r_f}{4E_f} [(\sigma_{P,c} - \sigma_{z,\Delta T}) \frac{4\tau l}{r_f} - \frac{8\tau^2 l^2}{r_f^2}] \quad (8)$$

where  $\sigma_{P,c}$  is the critical applied stress necessary for crack advance, and  $E_f$  is the Young's modulus of the fiber.

Substituting equations (6), (7) and (8) into equation (2) gives the  $G_{IIc}$ :

$$G_{IIc} = \frac{r_f}{4E_f} [(\sigma_{P,c} - \frac{4\tau l}{r_f})^2 - (\sigma_{z,\Delta T} - \frac{2\tau l}{r_f})^2] \quad (9)$$

Compared with Kalton's model (equation (10)), in which interfacial debonding initiates at the top of the specimen<sup>[21]</sup>, it is clear that there is some difference between equations (9) and (10) because the axial stress distribution in the fiber is different for the two situations of crack initiation at the bottom and crack initiation at the top.

$$G_{IIc} = \frac{r_f}{4E_f} (\sigma_{P,c} - \frac{2\tau l}{r_f} - \sigma_{z,\Delta T})^2 \quad (10)$$

## 2 Discussions

A set of parameters listed in Table 1 is employed to examine the predictions of the models presented above. All these materials are the common TMCs. The following analysis is based on equation (9). During push-out test, interfacial crack will advance as the strain energy release rate  $G_{II}$  provided by driving force reaches  $G_{IIc}$ , the interfacial fracture energy, at the crack tip. For a given value of  $G_{IIc}$ , the critical applied stress  $\sigma_{P,c}$  necessary for crack growth can be solved by equation (9), as shown in Fig. 4,  $\sigma_{P,c}$  is plotted as a function of  $G_{IIc}$  for the three different crack lengths. Clearly, the  $\sigma_{P,c}$  required for crack advance grows continually as  $G_{IIc}$ , and the stress required at the crack tip increases with the increasing of the crack length. It is caused by increased shielding of the crack tip provided by the frictional resistance to sliding.

The relationship of  $\sigma_{P,c}$  and crack length is plotted in Fig. 5 in four situations, namely, reference case,  $G_{IIc} = 40 \text{ J/m}^2$ ,  $\sigma_{z,\Delta T} = -800 \text{ MPa}$  and  $\tau_0 = -100 \text{ MPa}$ . It can be seen that  $\sigma_{P,c}$  required for crack advance will become greater when one of  $G_{IIc}$ ,  $\sigma_{z,\Delta T}$  and  $\tau$  rises. An increase in  $G_{IIc}$  inhibits crack growth, while increased frictional sliding resistance enhances the crack shielding effect. At the top end, the increased  $\sigma_{z,\Delta T}$  in the fiber needs larger  $\sigma_{P,c}$  to inhibit the fiber to protrude the matrix. Among these factors, the critical applied stress is more sensitive to the interfacial frictional shear stress.

Table 1 Reference set of parameters used to examine predictions of the analytical model

$E_f/$ GPa	$r_f/$ $\mu\text{m}$	$\sigma_{z,\Delta T}/$ MPa	$\sigma_{r,\Delta T}/$ MPa	$\tau_0/$ MPa	$G_{IIc}/$ $\text{J m}^{-2}$	$l_0/$ $\mu\text{m}$	$\mu$
469	70	-500	-150	-50	20	10	0.3

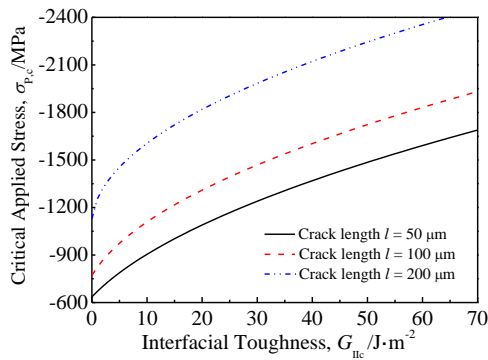


Fig.4 Critical applied stress necessary for crack growth, plotted as a function of interfacial toughness  $G_{IIC}$ , for three crack lengths

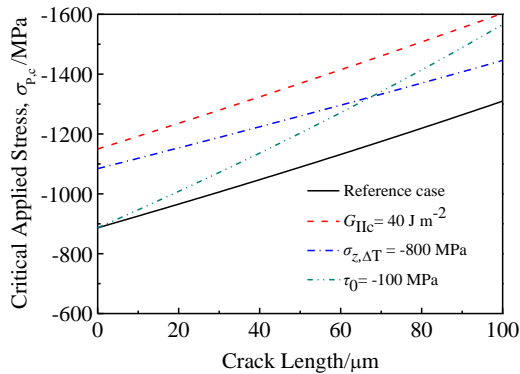


Fig.5 Influence, from  $G_{IIC}$ ,  $\sigma_{z,\Delta T}$  and  $\tau_0$ , on the applied stress necessary for crack advance as a function of crack length

It follows, if deduced values of the interfacial toughness are to be reliable, the preparing sample and push-out test must be operated cautiously and some experimental values such as the applied stress, the initial debonding length must be accurately measured.

### 3 Predictions and Validations

The model is applied to predict the push-out behavior of several TMCs. The thermo-elastic parameters of the fibers and titanium alloys<sup>[21,25-27]</sup> are listed in Table 2. The parametric values of the specimens, the thermal residual stresses  $\sigma_{z,\Delta T}$  and the experimental data required for the models<sup>[17,21,25,28]</sup> are shown in Table 3, where  $L$  denotes the thickness of specimen and  $l$  refers to the whole crack growth length. In this section, it is assumed that the  $l$  is 20  $\mu\text{m}$  and  $\mu$  is chosen to be 0.3.

The average thermal residual stresses are used since the specimen is thin, and are obtained by finite element method (ABAQUS). The analysis employs a fiber-matrix 2-D axisymmetric model, as shown in Fig.6a. In this model,

**Table 2 Thermo-elastic parameters of SiC and titanium alloy used in obtaining the thermal residual stresses by the finite element analysis and the interfacial toughness by the expressions from the model**

Material system	$E/\text{GPa}$	$\nu$	$\alpha/\times 10^{-6}$	Ref.
SCS-6	469	0.17	4.0	[25]
Sigma1240	400	0.21	4.0	[21]
Ti-6-4	115~30	0.36	7.3~10	[21]
Timetal 834	115~70	0.3	11.24	[25]
Timetal 21	98.2~40	0.35	6.81~9.5	[26,27]

**Table 3 Parameters of specimens, the thermal stresses obtained by the finite element analysis and data obtained from the push-out test**

Material system	$T/^\circ\text{C}$	$r_f/\mu\text{m}$	$L/\mu\text{m}$	$\sigma_{z,\Delta T}/\text{MPa}$	$P_{\max}/(\text{Exp.})$ [Ref.] N	$T/(\text{Exp.})$ [Ref.] MPa
Sigma1240/Ti-6-4	23	50	200	-318 <sup>[21]</sup>	8.1 <sup>[21]</sup>	-127
Sigma1240/Ti-6-4	600	50	200	-21 <sup>[21]</sup>	3.7 <sup>[21]</sup>	-28.7
SCS-6/Ti-6-4	23	71	550	-815	28 <sup>[28]</sup>	-448.6
SCS-6/Timetal 834	23	71	400	-839	31 <sup>[26]</sup>	-717.3
SCS-6/Timetal 834	530	71	400	-175	9.1 <sup>[26]</sup>	-141
SCS-6/Timetal 21s	23	70	530	-736	24 <sup>[17]</sup>	-379.7

**Table 4 Interfacial toughness simulated by other workers and calculated by Kalton's equation (3) and equation (9)**

Material System	$T/^\circ\text{C}$	$G_{IIC}/(\text{Simulation})$ $\text{J m}^{-2}$	$G_{IIC}/(\text{Kalton})$ $\text{J m}^{-2}$	$G_{IIC}/(\text{Eq. 9})$ $\text{J m}^{-2}$
Sigma1240/Ti-6-4	23		11.6	19.9
Sigma1240/Ti-6-4	600		5.57	5.51
SCS-6/Ti-6-4	23	52.5 <sup>[30]</sup>	18.6	48.4
SCS-6/Timetal 834	23	40 <sup>[25]</sup>	19.4	42.9
SCS-6/Timetal 834	530	5 <sup>[25]</sup>	3.9	6.2
SCS-6/Timetal 21s	23	50-70 <sup>[17]</sup>	13.7	37.26

the fiber and matrix are described with 4-nodes axisymmetric elements while the interface defined with 4-nodes cohesive elements generated by duplicating nodes at the interface on fiber and matrix sides. The fiber and matrix element size selected in both  $r$ -direction and

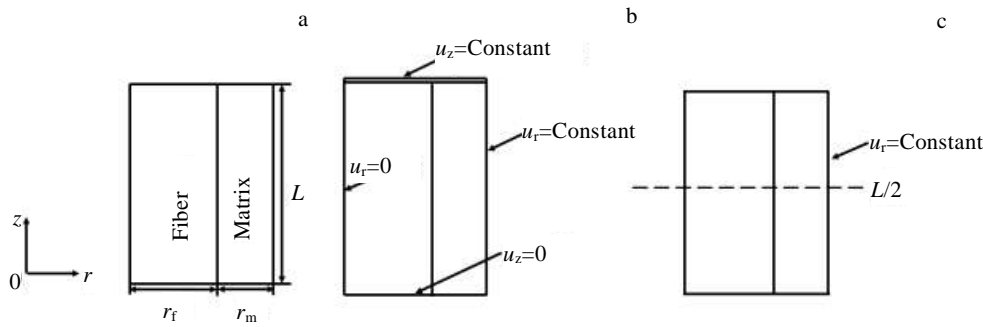


Fig.6 Axisymmetric finite element model (a), boundary conditions of the first step (b), and the boundary conditions of the second step (c)

$z$ -direction are  $2\ \mu\text{m}$ . The interphase element size in  $r$ -direction is 0 thickness, and is  $2\ \mu\text{m}$  in  $z$ -direction. The finite element analysis involves two major steps. The boundary conditions in the two steps are shown in Fig 6b and 6c. In the first step, the stress-free temperature of the alloy Ti-6Al-4V<sup>[21]</sup>, Timetal 834<sup>[25]</sup> and Timetal 21s<sup>[29]</sup> selected are 800, 770, and 875 °C, respectively.

The interfacial frictional shear stress  $\tau$  can be evaluated by the experimental data and the following equations

$$\tau = -\frac{1}{2\pi r_f} \frac{dP}{dz} \quad (11)$$

where  $dP/dz$  is the slope of the approximately linear region of the load/displacement curve in the push-out test.

Then the simulated results and other values in Table 3 are substituted into Equ.(9) and the results<sup>[17,25,30]</sup> calculated are listed in Table 4. As expected, the  $G_{IIC}$  values of the composites SCS-6/Ti-6Al-4V and SCS-6/Timetal 834 are in good agreement with the previous simulated data, while, for the composite SCS-6/Timetal 21s, there is a significant difference in the two results (present and previous), it may be induced by the error of  $\tau$  which is caused owing to the incomplete push-out load/displacement curve. The results from the present models are higher than that of those calculated by Kalton's equation (3). Apparently, it is not adequate to evaluate  $G_{IIC}$  of TMCs for the case of crack initiation at the bottom by the model for the crack initiation at the top since the axial stress distribution in the fiber in every region is different in the two cases.

#### 4 Conclusions

1) The model for single fiber push-out test, in which debonding initiates at the bottom of the samples, is developed to evaluate the interfacial fracture toughness  $G_{IIC}$  of TMCs. The solution to  $G_{IIC}$  is different from that for the case of crack initiation at the top since the axial stress distributions are different in the fiber. The critical applied stresses necessary for crack growth increases with

increasing the crack length, interfacial fracture toughness, interfacial frictional shear stresses and axial thermal residual stress.

2) In order to validate the predictions of the models, the interfacial fracture toughness of the composites Sigma1240/Ti-6-4, SCS/Ti-6-4, SCS/Timetal 834 and SCS/Timetal 21s are obtained by applying the  $G_{IIC}$  solutions, and the predictions are in good agreement with finite element analysis results. Thus, the models can be used to predict the interfacial toughness of TMCs for the cases where crack initiate at the bottom of the specimens.

#### References

- 1 Thomas M P, Winstone M R. *Composites Science and Technology*[J], 1999, 59: 297
- 2 Yuan Meini, Yang Yanqing, Huang Bin et al. *Transactions of Materials and Heat Treatment*[J], 2012, 33(6): 176 (in Chinese)
- 3 Yuan Meini, Yang Yanqing. *Rare Metal Materials and Engineering*[J], 2008, 37(12): 2104
- 4 Yang Y Q, Dudek H J, Kumpfert J. *Materials Science and Engineering A*[J], 1998, 246: 213
- 5 Yuan Meini, Yang Yanqing, Huang Bin et al. *Rare Metal Materials and Engineering*[J], 2009, 38(8): 1321
- 6 Mukherjee S, Ananth C R, Chandra N. *Scripta Materialia*[J], 1997, 36(11): 1333
- 7 Zeng Weidong, Zhou Yigang, Peters P W M. *Rare Metal Materials and Engineering*[J], 2002, 31(6): 445 (in Chinese)
- 8 Ananth C R, Chandra N. *Journal of Composite Materials*[J], 1995, 29: 1488
- 9 Chandra N, Ghonem H. *Composites: Part A*[J], 2001, 32: 575
- 10 Yuan Meini, Yang Yanqing, Ma Zhijun et al. *Rare Metal Materials and Engineering*[J], 2007, 36(6): 1115 (in Chinese)
- 11 Honda K, Kagawa Y. *Acta Materialia*[J], 1996, 44: 3267
- 12 Galbraith J M, Rhyne E P, Koss D A et al. *Scripta Materialia*[J], 1996, 35: 543
- 13 Rhyne E P, Hellmann J R, Galbraith J M et al. *Scripta Metallurgical Materialia*[J], 1995, 32: 547
- 14 Chandra N, Ananth C R. *Composites Science and*

- Technology[J], 1995, 54: 87
- 15 Yuan M N, Yang Y Q, Ma Z J. *Scripta Materialia*[J], 2007, 56: 533
- 16 Yuan Meini, Yang Yanqing, Huang Bin et al. *Transactions of Nonferrous Metals Society of China*[J], 2008, 18: 925
- 17 Mukherjee S, Ananth C R, Chandra N. *Composites: Part A*[J], 1998, 29: 1213
- 18 Ananth C R, Voleti S R, Chandra N. *Composites: Part A*[J], 1998, 29: 1203
- 19 Zhou L M, Mai Y W, Ye L. *Composites Engineering*[J], 1995, 5(10-11): 1199
- 20 Majumdar B S, Miracle D B. *Key Engineering. Materials*[J], 1996, 116/117: 153
- 21 Kalton A F, Howard S J, Janczak-Rusch J et al. *Acta Materialia*[J], 1998, 46: 3175
- 22 Jero P D, Kearns R J. *Scripta Metallurgical*[J], 1990, 24: 2315
- 23 Warren P D, Mackin T J, Evans A G. *Acta Metallurgical Materials*[J], 1992, 40: 1243
- 24 Liang C, Hutchinson J W. *Mechanics of Materials*[J], 1993, 14: 207
- 25 Zeng W D, Peters P W M, Tanaka Y. *Composites: Part A*[J], 2002, 33: 1159
- 26 Zheng D, Ghonem H. *Metallurgical and Materials Transactions A*[J], 1995, 26: 2469
- 27 Nyakana S L, Fanning J C, Boyer R B. *Journal of Materials Engineering and Performance*[J], 2005, 14: 799
- 28 Roman I, Jero P D. *MRS Proceedings*[J], 1992, 273: 337
- 29 Mukherjee S, Ananth C R, Chandra N. *Composites Science and Technology*[J], 1997, 57: 1501
- 30 Chandra N. *Composites: Part A*[J], 2002, 33: 1433

## Appendix

The displacement of the loading point is given, as following

$$\delta = \delta_1 + \delta_2 + \delta_3 = \frac{1}{E_f} \int_L^{L-l} \frac{2\tau(L-z)}{r_f} dz + 0 + \frac{1}{E_f} \int_{l_1}^0 (\sigma_{P,c} - \sigma_{z,\Delta T}) dz \quad (1a)$$

It followed that, here  $l_1 \approx L-l$ ,

$$d\delta = d\delta_1 + d\delta_2 + d\delta_3 = \frac{\pi r_f^2}{E_f} (\sigma_{P,c} - \sigma_{z,\Delta T} - \frac{2\tau l}{r_f}) dl \quad (1b)$$

$P = \sigma_{P,c} \pi r_f^2$ , the work done by the loading system is

$$dU_{ex} = Pd\delta = \frac{\pi r_f^2}{E_f} \sigma_{P,c} (\sigma_{P,c} - \sigma_{z,\Delta T} - \frac{2\tau l}{r_f}) dl \quad (1c)$$

Similarly, we obtained

$$U_{se} = \int_L^{L-l} \frac{1}{2} \varepsilon_1^z(z) \sigma_1^z(z) dV + 0 + \int_{l_1}^0 \frac{1}{2} \varepsilon_{III}^z(z) \sigma_{III}^z(z) dV \quad dV = \pi r_f^2 dz \quad (2a)$$

$$dU_{se} = \frac{\pi r_f^2}{2E_f} [(\sigma_{P,c} - \sigma_{z,\Delta T})^2 - \frac{4\tau^2 l^2}{r_f^2}] dl \quad (2b)$$

The term  $U_{fr}$  is

$$U_{fr} = \int_{Area} |\tau| \cdot |\nu(z)| dA \quad (3a)$$

$$\nu(z) = \int_{L-l}^z (\varepsilon_{final} - \varepsilon_{initial}) dz = \int_z^{L-l} [\frac{2\tau(L-z)}{r_f} - (\sigma_{P,c} - \sigma_{z,\Delta T})] dz \quad (3b)$$

$$\nu(z) = \frac{1}{E_f} \left\{ \frac{\tau}{r_f} [(L-z)^2 - l(L+l)] - (\sigma_{P,c} - \sigma_{z,\Delta T})(L-l-z) \right\} \quad (3c)$$

It is noted that the A.3d is valid when the equation A.3c is satisfied

$$|\sigma_{P,c} - \sigma_{z,\Delta T}| \geq \left| -\frac{2\tau l}{r_f} \right| \quad (3d)$$

The  $U_{fr}$  is obtained by substituting equation 3b into 3a, as follows

$$U_{fr} = \frac{2\pi r_f}{E_f} \int_L^{L-l} |\tau| \cdot \left| \frac{\tau}{r_f} [(L-z)^2 - l(L+l)] - (\sigma_{P,c} - \sigma_{z,\Delta T})(L-l-z) \right| dz \quad (3e)$$

$$dU_{fr} = \frac{\pi r_f^2}{2E_f} [(\sigma_{P,c} - \sigma_{z,\Delta T}) \frac{4\tau l}{r_f} - \frac{8\tau^2 l^2}{r_f^2}] dl \quad (3f)$$

## 纤维增强钛基复合材料界面断裂韧性的顶出法研究

孙庆<sup>1,2</sup>, 杨延清<sup>1</sup>, 罗贤<sup>1</sup>, 张荣军<sup>1</sup>, 黄斌<sup>1</sup>, 薛春岭<sup>1</sup>

(1. 西北工业大学凝固技术国家重点实验室, 陕西 西安 710072)

(2. 宝鸡文理学院, 陕西 宝鸡 721000)

**摘要:** 为了估计单向SiC纤维增强钛基复合材料的界面断裂韧性 $G_{Ic}$ , 提出了一个关于单根纤维顶出试验的新模型。在该模型中, 界面脱粘开始于试样的底端面。以断裂力学为基础推导出了 $G_{Ic}$ 的理论公式, 并且讨论了几个关键因素对 $G_{Ic}$ 的影响, 如裂纹扩展所需的外加应力, 裂纹长度以及界面的摩擦剪切应力。并且运用此模型预测了复合材料 Sigma1240/Ti-6-4, SCS/Ti-6-4, SCS/Timetal 834 和 SCS/Timetal 21s 的界面断裂韧性, 并与以前的有限元结果进行了比较。结果显示, 对于脱粘起始于试样的底端面的顶出试验, 该模型能较可靠地预测钛基复合材料的界面断裂韧性。

**关键词:** 钛基复合材料; 界面断裂韧性; 顶出试验; 剪滞方法

---

作者简介: 孙庆, 女, 1980年生, 博士, 西北工业大学凝固技术国家重点实验室, 陕西 西安 710072, 电话: 029-88486091, E-mail: sunq2009@126.com